Stage-III Annealing in Gold after Electron Irradiation*

C. LEE† AND J. S. KOEHLER
Department of Physics and Materials Research Laboratory, University of Illinois, Urbana, Illinois
(Received 13 June 1968)

Gold specimens of nominal 99.9999% purity were irradiated with 3-MeV electrons near liquid-nitrogen temperature. The damage production rate is found to depend on the purity of the specimen giving a lower value for the high-purity specimens. It is also found that the production rate is reduced remarkably by quenching the specimen before irradiation. For high-purity gold, a single large annealing peak is observed in stage III. The slope-change method and Primak analysis are employed to obtain the activation energy of stage-III annealing. Both methods give 0.85±0.02 eV for the activation energy in high-purity irradiated specimens. The activation energies for quenched and for quench-plus-irradiated specimens of comparable purity are found to be 0.85±0.03 and 0.86±0.02 eV, respectively, agreeing with the value for the irradiated specimens within the experimental error. Somewhat lower values are obtained for specimens of lower purity. Second-order kinetics are obeyed in the main part of the stage-III annealing for the irradiated, quench-plus-irradiated, and quenched specimens. Various models are discussed to explain stage-III annealing. It is concluded that vacancy migration in stage III with interstitial clusters acting as sinks can account for the observed results most satisfactorily in the case of gold.

I. INTRODUCTION

STAGE-III annealing occurs in irradiated noble metals in the temperature range from about 220 to 400°K. The atomic process responsible for the annealing has been the subject of considerable discussion. The present research on gold is an attempt to settle this question at least in the case of gold.

Stage-III recovery of the electrical resistivity of pure gold after irradiation has been investigated by several authors. Dworschak, Herschbach, and Koehler[1] irradiated 99.999% pure gold at 110°K with 10-MeV protons. They obtained an annealing activation energy of 0.80±0.04 eV for stage III using slope change and also using the Primak analysis. Bauer and Sosin[2] irradiated 99.999% pure gold near 80°K using 2-MeV electrons. They obtained 0.80±0.04 eV using the Meechan-Brinkman analysis. Dworschak *et al.* suggested the possibility that vacancy migration to interstitial clusters is responsible for stage-III annealing in gold. Bauer and Sosin claimed that stage-III annealing results from the migration of an interstitial to immobile vacancies.

So far, not enough data have been obtained to establish a definite model which can explain all of the phenomena observed during stage-III annealing in all fcc metals. Various models have been proposed to explain the recovery in stage III. The following possibilities have been suggested: (i) migration of a vacancy to interstitial clusters, (ii) migration of a second kind of interstitial to immobile vacancies, (iii) breaking up of interstitial clusters, (iv) migration of a di-interstitial to immobile vacancies, and (v) release of interstitials from the trap sites (impurities).

The purpose of this work is to obtain sufficient data to clarify the annealing mechanism of stage III using the purest gold available (99.9999%). To accomplish this, special attention has been directed to the following points:

(a) The determination of accurate activation energies employing several different methods of analysis.

(b) The dependence of the activation energy on the purity of the specimen.

(c) A comparison of activation-energy values obtained from irradiated, quenched, and quenched plus irradiated specimens to see if they differ.

(d) The determination of the order of the annealing kinetics for the irradiated, quenched plus irradiated, and quenched specimens.

(e) The determination of the number of jumps required for a migrating defect to anneal out for these three different experiments.

(f) The dependence of activation energy on the defect concentration.

II. EXPERIMENTAL PROCEDURE

A. Specimen Preparation and Mounting

The gold specimens used in this experiment were of 99.9999% purity supplied by Cominco. Specimens were prepared in two forms: strip of 5 mil thickness and of 36 mil width, and wire of 8 mil diam. Specimens were first spot-welded to the frame in zigzag form as described by Dworschak *et al.*[1] They were then cleaned with benzene and ethyl alcohol, etched with *aqua regia*, and rinsed thoroughly twice with distilled water. Then they were put into a ceramic boat and annealed for 3 h at 900°C in an open-air furnace. The residual resistivity of the specimens annealed in this manner ranged from 0.47 to 0.67×10^{-9} Ω cm for the strip and from 0.89 to 1.1×10^{-9} Ω cm for the wire. These resistivity values and the bulk values after size correction are listed in columns 2 and 3 of Table I. After annealing some of the specimens were quenched from 700°C to water near 0°C. The quenched-in resistivities ranged from 2.4 to 5.1×10^{-9} Ω cm. The quenching rate was (5×10^{4})°C/sec.

* This research was supported in part by the U. S. Atomic Energy Commission under Contract No. AT(11-1)-1198.
† Present address: University of Montreal, Montreal, Canada.
[1] F. Dworschak, K. Herschbach, and J. S. Koehler, Phys. Rev. 133, A292 (1964).
[2] W. Bauer and A. Sosin, Phys. Rev. 136, A474 (1964).

TABLE I. Residual resistivity and damage-production data.

Specimen number	Residual resistivity before size correction (10^{-9} Ω cm)	Residual resistivity after size correction[a] (10^{-9} Ω cm)	Resistivity change by irradiation (10^{-9} Ω cm)	Resistivity change by quench (10^{-9} Ω cm)	Total electron flux (10^{17} el/cm^2)	Quenching temperature (°C)	Type of specimen	Remarks
I-1	1.010	0.388	4.237	···	7.1	···	wire	front
I-2	0.499	0.127	2.444	···	7.1	···	strip	back
II-1	1.096	0.481	4.528	···	7.5	···	wire	front
II-2	0.498	0.126	2.400	···	7.5	···	strip	back
III-1	1.072	0.454	1.246	···	3.3	···	wire	back
III-2	0.563	0.173	2.072	···	3.3	···	strip	front
IV-1	0.901	0.273	4.499	···	7.5	···	wire	front
IV-2	0.581	0.188	2.437	···	7.5	···	strip	back
VII-1	0.968	0.344	5.361	···	12.5	···	wire	front
VII-2	0.469	0.107	2.866	···	12.5	···	strip	back
VIII-1	1.045	0.426	4.715	···	7.5	···	wire	front
VIII-2	0.504	0.131	1.852	···	7.5	···	strip	back
IIIX-1	0.996	0.373	0.409	···	0.31	···	wire	front
IX-2	0.490	0.121	0.245	···	0.31	···	strip	back
X-1	1.026	0.405	0.117	···	0.12	···	wire	back
X-2	0.538	0.155	0.225	···	0.12	···	strip	front
XI-2	0.522	0.143	···	2.42	···	730	strip	quench only
XII-1	0.955	0.330	···	2.71	···	690	wire	quench only
XIII-1	0.947	0.321	5.200	···	22.5	···	wire	back
XIII-2	0.900	0.272	1.737	2.91	22.5	710	wire	front, Q+R
XIV-1	0.545	0.160	0.613	3.37	10.2	700	strip	front, Q+R
XIV-2	0.674	0.264	3.613	···	10.2	···	strip	back
XVII-1	0.545	0.160	0.668	3.80	7.1	710	strip	front, Q+R
XVII-2	0.552	0.165	8.338	···	38.7	···	strip	back
XVIII-1	0.929	0.302	5.299	···	19.5	···	wire	back
XVIII-2	0.910	0.282	1.292	3.61	19.5	710	wire	front, Q+R
XX-1	0.960	0.335	10.459	···	25.4	···	wire	front
XX-2	0.555	0.167	7.652	···	25.4	···	strip	back
XXI-1	0.533	0.151	8.499	···	32.0	···	strip	front
XXI-2	0.897	0.269	6.778	···	32.0	···	wire	back

[a] Size corrections are done by using equations given in the article by E. H. Sondheimer, Advan. Phys. 1, 1 (1952), and the value of the product of the bulk resistivity and free path by R. G. Chambers, Proc. Roy. Soc. (London) **A215**, 481 (1952). See Sec. IV E for the discussion on the size correction.

The specimens were mounted on an aluminum block in the manner described by Dworschak *et al.*[1] Two specimens were mounted in a block, one on the front side, the other on the back side. A vacuum seal was achieved using indium O rings. Irradiation windows in the cover plates on both sides of the block were made of Duralumin foil of thickness 1.5 mil.

B. Irradiation Procedure

A 3-MeV electron beam from the Van de Graaff at the Materials Research Laboratory, University of Illinois, was used to irradiate the specimens. The liquid-nitrogen cryostat used in this experiment was the one used by Lwin *et al.*[3] and similar irradiation procedure was followed.

The temperature of the specimen was kept below 110°K throughout the irradiation. The temperature was monitored by a copper-constantan thermocouple with the test junction spot-welded to a dummy specimen and the reference junction at liquid nitrogen. Throughout the run, the temperature was recorded by using a millivolt recorder. The total electron flux at the Faraday cage ranged from 10^{16} electrons/cm^2 for a low dose to 4×10^{18} electrons/cm^2 for a high dose.

C. Measurements and Annealing

Standard potentiometric methods were employed for the measurement of resistivity using a Rubicon 6 Dial Potentiometer. Using 4 A of measuring current, the uncertainty of the resistivity measurements was less than $\pm3\times10^{-13}$ Ω cm. The excellent stability of the measurement was obtained by immersing the specimen block deep into liquid helium (more than 1 ft), and by allowing 7 to 10 min of time to elapse before making measurements. The space inside the specimen block was connected to a large tank of helium gas at about 3 lb/in.^{2} pressure, with rubber tubing. When the specimen block was immersed in liquid helium, the gas pressure dropped to near zero, indicating that most of the helium gas was condensed into liquid helium.

With 4 A passing through the specimen in liquid helium, no appreciable rise in pressure was observed, which indicated that the temperature of the specimen was kept close to liquid-helium temperature during the resistivity measurement.

Annealing was carried out in a constant temperature bath, using three different kinds of liquids: Mixture

[3] See, for example, Y. Lwin, Ph.D. thesis, University of Illinois, 1967 (unpublished); see also Y. N. Lwin, M. Doyama, and J. S. Koehler, Phys. Rev. **165**, 787 (1968).

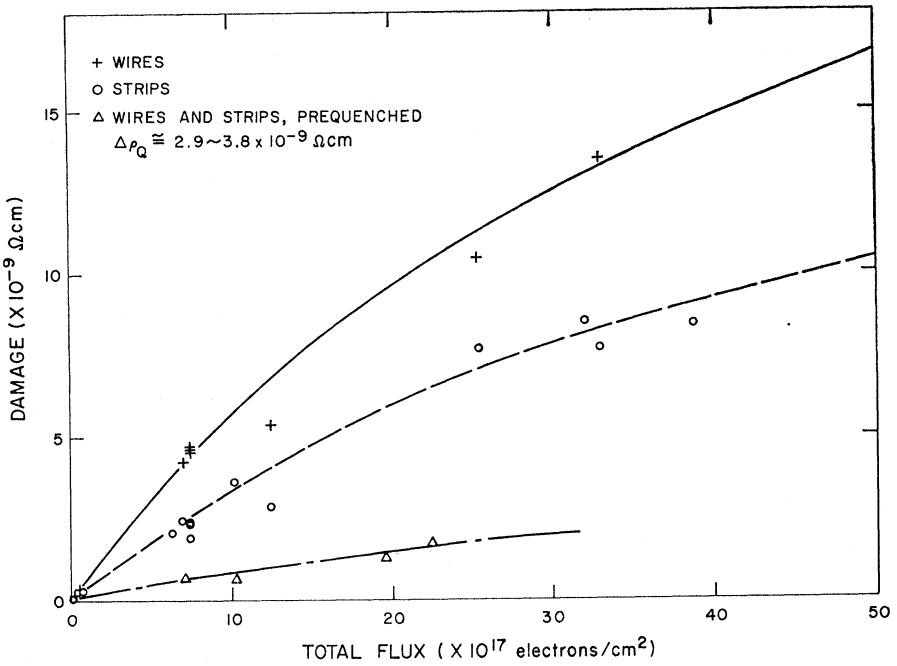

FIG. 1. Damage-production curves for pure gold by 3-MeV electron irradiation. The upper curve is the result for the wire specimens, the middle curve for the strips, and the lower curve for the prequenched specimens. The results for the prequenched specimens are for both wires and strips.

No. 39 [4] was used from −130 to 20°C, deionized water between 30 to 90°C, and benzyl alcohol from 100 to 150°C. The temperature of the annealing bath was controlled and maintained constant to within ±0.01°C by an electric heater wound around a cylinder and a coolant (liquid nitrogen or ice water) outside of the bath. Helium exchange gas was used between the bath and the coolant. The temperature of the bath was measured by a Leeds and Northrup platinum resistance thermometer calibrated by the U. S. National Bureau of Standards.

A time correction for annealing was always made because the time required to reach equilibrium temperature was not negligible. This will be discussed later in more detail. The temperature difference between the bath and the specimen was monitored by the copper-constantan thermocouple and was recorded with a Leeds and Northrup dc amplifier and a microvolt recorder.

III. EXPERIMENTAL RESULTS

A. Damage Production

The results of damage production by irradiation and by quenching are listed in Table I. Figure 1 shows the damage production curves for the irradiated specimens. As one can see, the curves bend down as the dose increases. There are significant differences in the production rate between the wire and the strip. Thus the production rate depends strongly on the purity of the specimen; i.e., the purer the specimen, the less damage production results. Every datum point in Fig. 1 represents a different specimen. The scattering of points in Fig. 1 is, therefore, due at least partially to the difference in purity of the specimens.

As one can see from Table I and Fig. 1, the damage production rate is reduced remarkably by quenching the specimen before irradiation. The damage rate for the prequenched specimens is only $\frac{1}{3}$ to $\frac{1}{6}$ of the rate for the unquenched specimens. This means that interstitials move at nitrogen temperature, and are annihilated at lattice vacancies. The last column of Table I shows whether the specimen is in the front or in the back during irradiation. The production rate for the front specimen is considerably higher than that for the back specimen. This means that the electrons are scattered appreciably during their passage through the specimen. Consequently, the actual electron flux which hits the specimen is somewhat larger than that collected in the Faraday cup.

B. Isochronal Annealing

Some typical isochronal annealing curves are shown in Fig. 2. Except for block VII, all annealing was done in steps of 10°C with 32-min pulses. Block VII was annealed in steps of 5°C with 10-min pulses. The differentials (slopes) of these isochronal curves are shown in Fig. 3.

The features of these graphs to be noted are:

(i) A large and broad single peak is observed in stage III. No small auxiliary peak on the lower-temperature side of the stage-III peak is observed, contrary to the

[4] Mixture of the following chemicals: chloroform ($CHCl_3$), 14.5 wt%; methylene chloride (CH_2Cl_2), 25.3 wt%; ethyl bromide ($C_2H_5B_2$), 33.4 wt%; trans-dichloroethylene ($C_2H_2Cl_2$), 10.4 wt%; trichloroethylene (C_2HCl_3), 16.4 wt%.

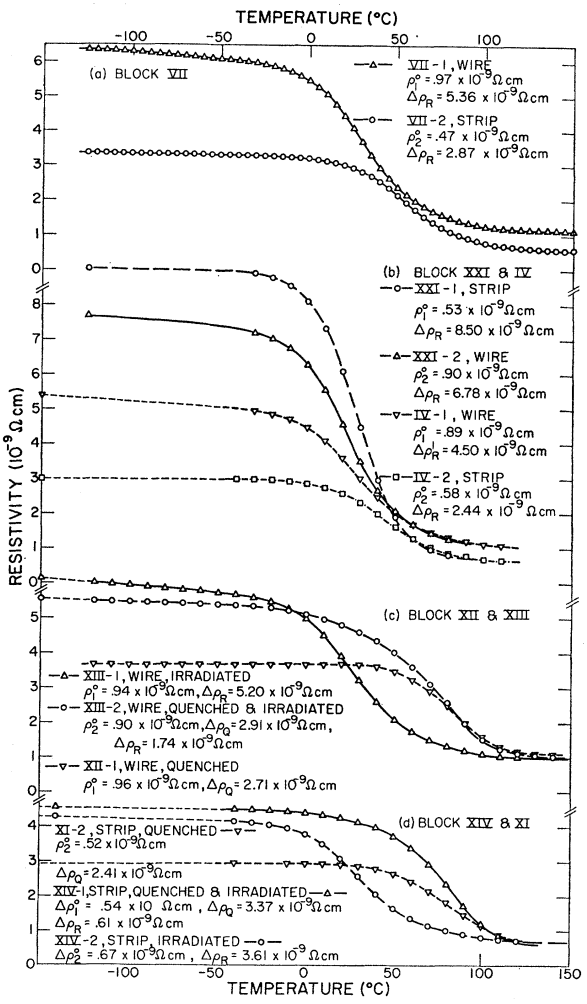

FIG. 2. (a) Isochronal annealing curves for block VII. (10-min pulses.) ρ^0 is the residual resistivity and $\Delta\rho_R$ is the resistivity increase by irradiation. (b) Isochronal annealing curves for blocks IV and XXI. (32-min pulses.) (c) Isochronal annealing curves for blocks XII and XIII (32-min pulses). The specimen XII-1 is quenched, XIII-1 is irradiated, and XIII-2 is quenched and then irradiated. $\Delta\rho_Q$ is the resistivity increase by quenching. (d) Isochronal annealing curves for blocks XI and XIV. (32-min pulses.) The specimen XI-2 is quenched, XIV-1 is quenched and irradiated, and XIV-2 is irradiated.

case of copper,[1] or silver.[1] Aluminum shows similar simplicity.[3]

(ii) The peak temperature for irradiated specimens lies between 25 and 30°C for the wire and 30 and 55°C for the strip. With the same damage, the peak temperature of the wire is lower than that of the strip. The peak temperature of the specimen with higher dose is shifted toward lower temperature.

(iii) The peak temperature for the quenched and the quenched-and-irradiated specimens are the same and is about 90°C in both cases.

(iv) In quenched-and-irradiated specimens, a small shoulder at about 60°C is observed on the low-temperature side of the main peak.

(v) The annealing below stage III is very small. The purer the specimen, the smaller is the annealing below stage III. For example, the fractional recovery below stage III for the specimen VII-2 ($\rho^0 = 0.469 \times 10^{-9}$ Ω cm) is 2.5%, while that for the specimen VII-1 ($\rho^0 = 0.968 \times 10^{-9}$ Ω cm) is 7%. The recovery below stage III for the specimens used by Bauer and Sosin[2] is about 25% for a specimen, with $\rho^0 = 2.6 \times 10^{-9}$ Ω cm having about the same initial damage as VII-2 and VII-1.

(vi) At the end of stage III (ranging from 80 to 130°C), practically all the damage is annealed out. The remaining defect resistivity after stage III is in the range of 1 to 3% of the initial defect resistivity for the irradiated specimens. In contrast, the corresponding

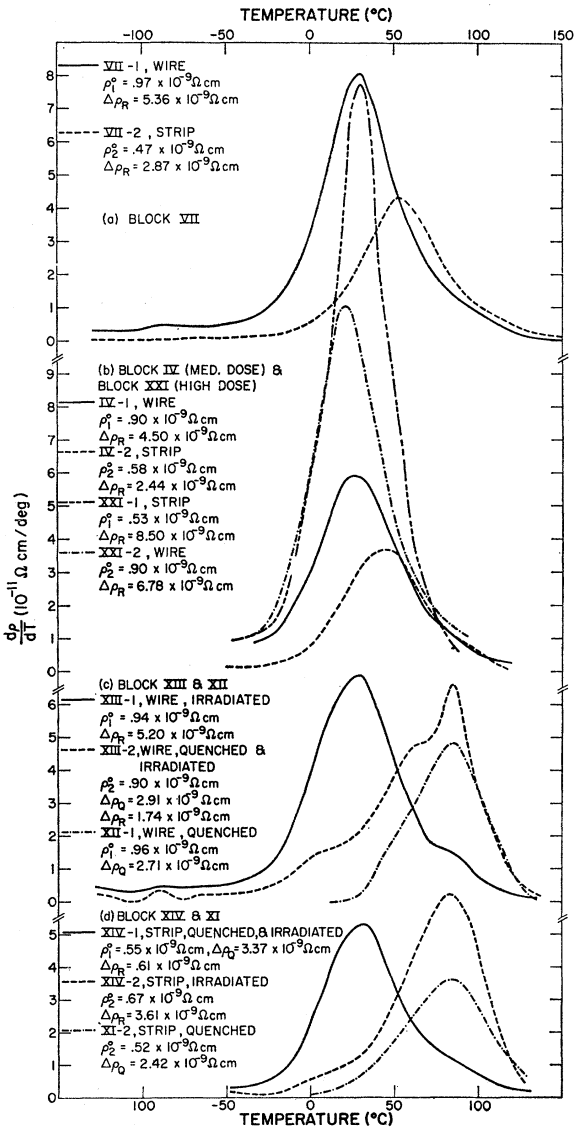

FIG. 3. (a) Slopes of isochronal curves for block VII. (b) Slopes of isochronal curves for blocks IV and XXI. (c) Slopes of isochronal curves for blocks XII and XIII. (d) Slopes of isochronal curves for blocks XI and XIV.

TABLE II. Activation energies obtained by slope-change and Primak method.

Specimen number	E^a (eV) by slope change	E^b (eV) by Primak	$\bar{E}$ (eV)	$\Delta E/\bar{E}^c$ (%)	Remarks
I-1	0.841±0.049(0.850)	0.808±0.016	0.825±0.033	4.0	wire, medium dose
I-2	0.861±0.038(0.897)	0.849±0.017	0.855±0.028	1.4	strip, medium dose
IV-1	0.837±0.044(0.828)	0.829±0.017	0.833±0.031	1.2	wire, medium dose
IV-2	0.844±0.020(0.841)	0.858±0.018	0.851±0.019	1.6	strip, medium dose
VII-1	···	0.815±0.020	0.815±0.020	···	wire, medium dose
VII-2	···	0.867±0.020	0.867±0.020	···	strip, medium dose
VIII-1	···	0.818±0.018	0.818±0.018	···	wire, medium dose
VIII-2	···	0.850±0.018	0.850+0.018	···	strip, medium dose
XI-2	0.861±0.015(0.867)	0.851±0.020	0.856±0.018	1.2	strip, quench only
XII-1	0.883±0.034(0.927)	0.859±0.020	0.871±0.027	2.8	wire, quench only
XIII-1	0.844±0.026(0.844)	0.822±0.017	0.833±0.022	2.6	wire, medium dose
XIII-2	0.860±0.043(0.864)	0.842±0.020	0.851±0.032	2.0	wire, quench+irrad.
XIV-1	0.858±0.018(0.866)	0.864±0.020	0.861±0.019	0.7	strip, quench+irrad.
XIV-2	0.845±0.021(0.856)	0.827±0.017	0.836±0.019	2.2	strip, medium high dose
XVII-1	···	0.850±0.020	0.850±0.020	···	strip, quench+irrad.
XVII-2	0.843±0.055(0.821)	0.845±0.018	0.844±0.037	0.2	strip, high dose
XXI-1	0.846±0.025(0.847)	0.855±0.017	0.851±0.021	1.1	strip, high dose
XXI-2	0.816±0.031(0.813)	0.825±0.016	0.821±0.024	1.1	wire, high dose

[a] These are average values at several temperatures near the peak. Energy values at the peak are also shown in parentheses.
[b] These are the values taken at the center of the peak of the activation energy spectra.
[c] $\Delta E = |E_{\text{slope change}} - E_{\text{Primak}}|$.

figure observed by Dworschak *et al.*[1] was about 14%, while that seen by Bauer *et al.*[2] was about 7%.

C. Isothermal Annealing

For the purpose of obtaining activation energies by Primak analysis and by the change of slope method, blocks I, IV, XI, XII, XIII, XIV, XVII, and XXI were annealed isothermally in temperature steps of 10°C ranging from −110 to 130°C. At each temperature, five measurements were made after 3, 6, 12, 22, and 32 min of annealing, respectively. (In some early measurements, 2-, 4-, 8-, 16-, and 32-min annealings were used instead.)

The timer measuring the annealing time was started when the specimen temperature reached 1°C below the bath temperature. The temperature difference was monitored and recorded by a dc amplifier and a microvolt recorder as described earlier. The annealing time was later corrected by calculating the equivalent time using the following relation and the graph of the temperature difference versus time recorded by microvolt recorder:

$$t' = t \exp\left[-\frac{E}{k}\left(\frac{T_0 - T}{TT_0}\right)\right], \quad T_0 > T$$

where t' is the equivalent time interval corrected for the bath temperature T_0, t is the actual time spent at temperature T, E is the activation energy, and k is the Boltzmann constant. The temperature-difference curves were divided into small intervals of time, the correction is made using the above equation, and finally these corrected time intervals were added to give the total time of annealing. The time correction for one annealing was less than 10 sec for the deionized water bath, about 15 sec for the mixture No. 39 bath, and about 20 sec for the benzyl alcohol bath.

Blocks II, VIII, and XVIII were annealed isothermally for a very long time (300 to 500 min) at several different temperatures in order to determine the order of kinetics.

D. Determination of Activation Energy

1. Change of Slope Method

The activation energy of a process can be obtained by measuring the change of the rate of the isothermal annealing after a sudden change of annealing temperature from T_1 to T_2. The activation energy is, then, given by

$$E = \frac{kT_1T_2}{T_2 - T_1} \ln\left(\frac{d\rho}{dt}\right)_{T=T_2} \Big/ \left(\frac{d\rho}{dt}\right)_{T=T_1}, \quad T_2 > T_1 \quad (3.1)$$

where $(d\rho/dt)_T$ is the slope of the isothermal curve at temperature T and k is the Boltzmann constant. The slopes are obtained graphically after time corrections are made: At first the slopes from the isothermal curves without time correction are obtained to calculate uncorrected activation energy. Using this uncorrected energy the time correction is made. Then the isothermal curve is replotted with time correction to get the correct slopes which are, in turn, used to calculate the final value of the activation energy. It is assumed in this method that the concentration of all defects is not altered when the temperature changes. Considerable care must be exercised in handling the data if this is not a valid assumption. The temperature changes $(T_2 - T_1)$ are kept small to ensure that this assumption will be valid. The results are listed in the second column of Table II.

2. Primak Analysis. The Activation Energy Spectra

The isothermal data used above can be used to obtain activation-energy spectra employing Primak analysis.

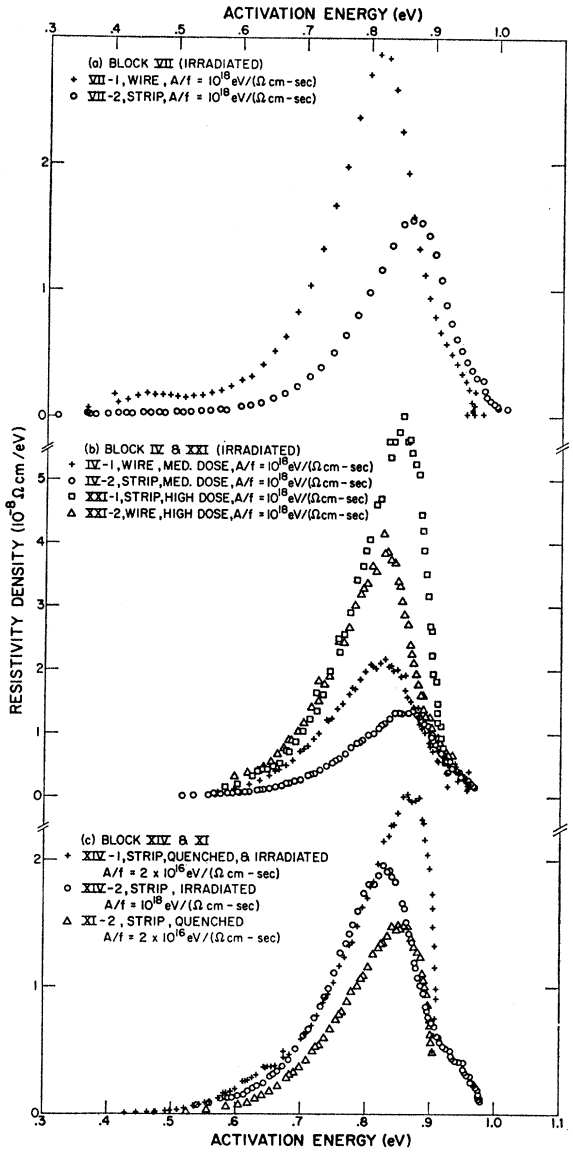

FIG. 4. (a) Activation-energy spectra for the specimens VII-1 (wire) and VII-2 (strip, medium dose). (b) Activation-energy spectra for the specimens IV-1 (wire, medium dose), IV-2 (strip, medium dose), XXI-1 (strip, high dose), and XXI-2 (wire, high dose). (c) Activation-energy spectra for the specimens XI-2 (strip, quenched), XIV-1 (strip, quenched and irradiated), and XIV-2 (strip, irradiation only).

Primak[5] first discussed in detail the annealing of kinetic processes distributed in activation energy. Since the recovery in stage III obeys essentially second-order kinetics (see next section), the distribution function (resistivity density) after the nth anneal can be written as[1]

$$P_{0l}(\bar{E})=\rho_n(t_n')-\rho_n(t_n'')\Big/\int_0^\infty I_n dE, \qquad (3.2)$$

where

$$I_n=\left[1+\frac{A}{f}P_{0l}\Big(\sum_{i=1}^{n-1} t_i e^{-E/kT_i}+t_n' e^{-E/kT_n}\Big)\right]^{-1}$$
$$-\left[1+\frac{A}{f}P_{0l}\Big(\sum_{i=1}^{n-1} t_i e^{-E/kT_i}+t_n'' e^{-E/kT_n}\Big)\right]^{-1}. \qquad (3.3)$$

$\rho_n(t_n)$ is the resistivity observed during the nth anneal at time t_n and $\bar{E}$ is the average activation energy during the nth anneal. $\bar{E}$ is defined by[6]

$$\bar{E}=\int_0^\infty EI_n dE\Big/\int_0^\infty I_n dE, \qquad (3.4)$$

A is a frequency factor including a capture volume σ and an entropy factor, and $f/100$ is the resistivity produced by 1% of defects (i.e., $A=\nu\sigma G$).

Starting with appropriate initial values of A/f and P_{0l}, Eq. (3.2) was solved by iteration. Iteration was continued until successive values of $P_{0l}(\bar{E})$ satisfy

$$|P_{0l}^{k+1}-P_{0l}^{k}|/P_{0l}^{k}<0.01,$$

where P_{0l}^{k} is the value after kth iteration. Numerical integrations were carried out with an IBM 7094 digital computer employing Gauss's mechanical quadrature formula.

The calculated activation energy spectrum was composed of many segments, one for each annealing temperature. The value of A/f was then varied successively until these segments joined together smoothly. The uncertainty in A/f determined in this manner was found to be a factor of 2, and the corresponding uncertainty in activation energy due to the change of A/f by this factor of 2 was less than 0.02 eV. Activation energy was then determined by reading the value of E at the center of the peak in the P_{0l} versus E curve. The values of activation energy obtained in this way are tabulated in Table II, and some typical results of activation-energy spectra are shown in Fig. 4.

As one can notice from these figures, there is a marked difference in the values of A/f between irradiated and quenched specimens. For the irradiated specimens, the best value of A/f is 10^{18} eV/Ω cm sec. This value agrees with that found by Dworschak *et al.*[1] For quenched and quench-plus-irradiated specimens, on the other hand, it is 2×10^{16} eV/Ω cm sec. The reason for this large difference will be discussed later.

The values of activation energy obtained by Primak analysis agree quite well with those found by the slope-change method as shown in Table II. The difference is less than a few percent.

[5] W. Primak, Phys. Rev. **100**, 1677 (1955); J. Appl. Phys. **31**, 1524 (1960).

[6] J. H. Bredt, Ph.D. thesis, University of Illinois, 1960 (unpublished).

3. Summary on the Activation Energy

The results on the activation energy are summarized below:

(*i*) *Average activation energy for irradiated specimens.* For the strips:

$\bar{E}_{\text{slope change}}=0.849\pm0.032$ eV (5 specimens, 48 measurements),
$\bar{E}_{\text{Primak}}=0.850\pm0.018$ eV (7 specimens).

For the wires:

$\bar{E}_{\text{slope change}}=0.835\pm0.038$ eV (4 specimens, 37 measurements),
$\bar{E}_{\text{Primak}}=0.821\pm0.017$ eV (6 specimens).

Taking the average over the values by Primak and slope-change methods,

$\bar{E}_{\text{strip}}=0.850\pm0.024$ eV,
$\bar{E}_{\text{wire}}=0.828\pm0.026$ eV.

(*ii*) *Activation energy for quenched specimens.*

$E_{\text{strip}}=0.856\pm0.018$ eV (1 specimen),
$E_{\text{wire}}=0.871\pm0.027$ eV (1 specimen).

(*iii*) *Activation energy for quench-plus-irradiated specimens.*

$E_{\text{strip}}=0.856\pm0.019$ eV (2 specimens),
$E_{\text{wire}}=0.851\pm0.032$ eV (1 specimen).

(*iv*) *Dependence of activation energy on purity.* As one notes from Table II, there is a rather systematic dependence of the activation energy on purity. The higher the purity, the higher is the activation energy. This result is shown in Fig. 5, where the activation energy of the specimens is plotted against the residual resistivity.

(*v*) *Dependence of activation energy on dose is not as remarkable as that on purity.* The average values for the strips with about the same purity are compared below for two different doses:

For the dose $\Delta\rho_R\cong2.4\times10^{-9}$ Ω cm,

$\bar{E}_{\text{medium dose}}=0.853\pm0.024$ eV (2 specimens).

For the dose $\Delta\rho_R\cong8.4\times10^{-9}$ Ω cm,

$E_{\text{high dose}}=0.847\pm0.029$ eV (2 specimens).

The residual resistivities for these specimens are about 0.54×10^{-9} Ω cm (0.16×10^{-9} Ω cm for the bulk resistivity). There are not enough data available for the wires.

E. Determination of the Order of Kinetics

The order of kinetics can be determined from the isothermal annealing data. For a second-order process, the solution of the rate equation can be written as

$$(\rho-\rho_\infty)^{-1}-(\rho_0-\rho_\infty)^{-1}=B\times(t-t_0)e^{-E/kT}, \quad (3.5)$$

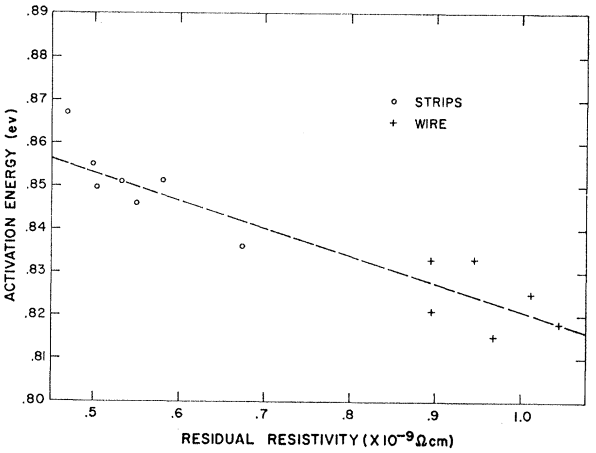

FIG. 5. Dependence of the activation energy on the purity of the specimen. Resistivities in the graph are actually measured values without size correction.

where ρ_0, ρ, and ρ_∞ are the resistivities at $t=t_0$, t, and ∞, respectively. E is the activation energy, k the Boltzman constant, T the absolute temperature, and B the constant which includes the frequency factor ν and capture volume. If one plots $(\rho-\rho_\infty)^{-1}$ against $t-t_0$, one would obtain a straight line according to Eq. (3.5). In the conventional method, one must assign an assumed value to ρ_∞ beforehand, and then vary it until one gets the best straight-line fit. Such a choice enables one to distort forcefully the original data by changing the value of ρ_∞ at will in order to get the best fit.

Therefore, another type of plot was devised. In this new method, the value of ρ_∞ is not assumed beforehand, but is determined from the graph. From Eq. (3.5), we can write

$$[(\rho-\rho_\infty)(\rho_0-\rho_\infty)/(\rho_0-\rho)]Be^{-E/kT}=(t-t_0)^{-1}.$$

Noting that $\rho-\rho_\infty=\rho-\rho_0+\rho-\rho_\infty$, we obtain, after some rearrangement,

$$(t-t_0)^{-1}=Be^{-E/kT}(\rho_0-\rho_\infty)^2(\rho_0-\rho)^{-1}-Be^{-E/kT}(\rho_0-\rho_\infty). \quad (3.6)$$

Define

$$\alpha\equiv Be^{-E/kT}(\rho_0-\rho_\infty)^2,\qquad \beta\equiv Be^{-E/kT}(\rho_0-\rho_\infty); \quad (3.7)$$

then Eq. (3.6) becomes

$$(t-t_0)^{-1}=\alpha(\rho_0-\rho)^{-1}-\beta. \quad (3.8)$$

If $(t-t_0)^{-1}$ is plotted against $(\rho_0-\rho)^{-1}$, we will get a straight line for a second-order process. From Eqs. (3.7),

$$\alpha/\beta=\rho_0-\rho_\infty, \quad \text{or} \quad \rho_\infty=\rho_0-\alpha/\beta. \quad (3.9)$$

Thus, by reading the values of α (slope of the straight line) and of β [intercept of the straight line at $(t-t_0)^{-1}$ axis] from the graph, one can get the value of ρ_∞. Figures 6 and 7 are some examples of the second-order plots obtained in this way.

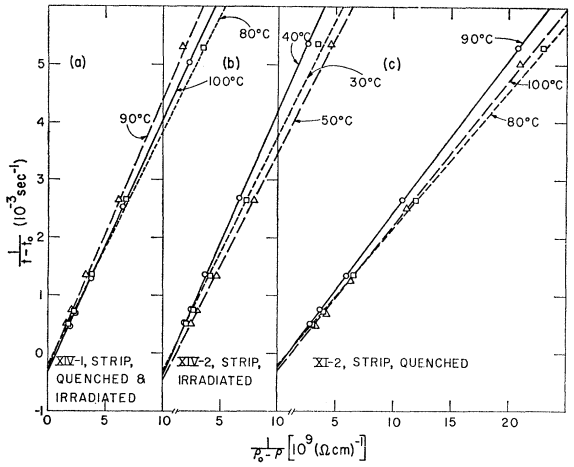

FIG. 6. (a) Second-order plot of the speciman XIV-1 at temperatures 80, 90, and 100°C. The peak is at 90°C. The ρ_∞ values are 0.8681×10^{-9}, 0.5082×10^{-9}, and 0.4096×10^{-9} Ω cm at 80, 90, and 100°C, respectively. (b) Second-order plot of the specimen XIV-2 at temperatures 30, 40, and 50°C. The peak is at 40°C. The ρ_∞ values are 1.6551×10^{-9}, 1.3943×10^{-9}, and 1.2184×10^{-9} Ω cm at 30, 40, and 50°C, respectively. (c) Second-order plot of the specimen XI-2 at temperatures 80, 90, and 100°C. The peak is at 90°C. The values of ρ_∞ are 0.9168×10^{-9}, 0.6321×10^{-9}, and 0.5816×10^{-9} Ω cm at 80, 90, and 100°C, respectively.

From the values of β and of $\rho_0-\rho_\infty$ at successive known temperatures T_1 and T_2, an activation energy E can be obtained in principle. From Eq. (3.7), one can write

$$E=\frac{KT_1T_2}{T_2-T_1}\ln\frac{\beta_{T_2}(\rho_0-\rho_\infty)_{T_1}}{\beta_{T_1}(\rho_0-\rho_\infty)_{T_2}},\quad T_2>T_1$$

or

$$E=\frac{KT_1T_2}{T_2-T_1}\ln\frac{\alpha_{T_2}(\rho_0-\rho_\infty)_{T_1}^2}{\alpha_{T_1}(\rho_0-\rho_\infty)_{T_2}^2},\quad T_2>T_1.$$

Unfortunately, the value of β is very difficult to determine accurately from the data, and since it enters into both methods for calculating E, the results show large fluctuations. We will therefore not use this method to determine E.

For a first-order process, we could not obtain a new formula with which we could get a unique plot without assuming and varying the value of ρ_∞. We used, therefore, the conventional method with which we varied the preassumed value of ρ_∞ until we get the best straight-line fit. Nowhere in stage III could we fit the annealing data to the first-order kinetics. Only at small peak near −90°C (stage II), which was observed for the wire specimens, could we get first-order kinetics (Fig. 8).

The following are the features observed:

(i) The second-order fit is good for most of the stage-III peak for both irradiated and quenched specimens. (ii) For the quench-plus-irradiated specimen, the annealing process near the peak center is still close to the second order. (iii) Near the foot of the peak on both sides, the annealing does not follow second-order kinetics, but is nearly 1.5 order. (iv) The annealing process near the small peak at −90°C (stage II) observed for the wire specimens follows first-order kinetics (Fig. 8). (v) The value of ρ_∞ decreases monotonically as annealing temperature increases.

IV. DISCUSSION OF RESULTS

A. Activation Energy and Interpretation of Stage III in Gold

The activation energies measured in the stage-III annealing of gold are summarized below:

For 3-MeV electron irradiated specimens:

$$\bar{E}_{\text{strip}}=0.85\pm0.02\text{ eV},\quad \rho^0\cong0.5\times10^{-9}\ \Omega\text{ cm},$$
$$\bar{E}_{\text{wire}}=0.83\pm0.03\text{ eV},\quad \rho^0\cong1.0\times10^{-9}\ \Omega\text{ cm},$$

where ρ^0 is the measured resistivity at 4.2°K before introduction of defects. No size correction has been made. For quenched plus electron irradiated specimens:

$$\bar{E}_{\text{strip}}=0.86\pm0.02\text{ eV},\quad \rho^0\cong0.5\times10^{-9}\ \Omega\text{ cm},$$
$$E_{\text{wire}}=0.85\pm0.03\text{ eV},\quad \rho^0\cong0.9\times10^{-9}\ \Omega\text{ cm}.$$

For quenched specimens:

$$E_{\text{strip}}=0.86\pm0.02\text{ eV},\quad \rho^0\cong0.5\times10^{-9}\ \Omega\text{ cm},$$
$$E_{\text{wire}}=0.87\pm0.03\text{ eV},\quad \rho^0\cong1.0\times10^{-9}\ \Omega\text{ cm}.$$

These activation energies are slightly higher than the values reported in earlier irradiation experiments[1,2] (about 0.05 eV higher) but the difference can be understood if allowance is made for the higher purity of the present specimens (see Sec. III B). The values are

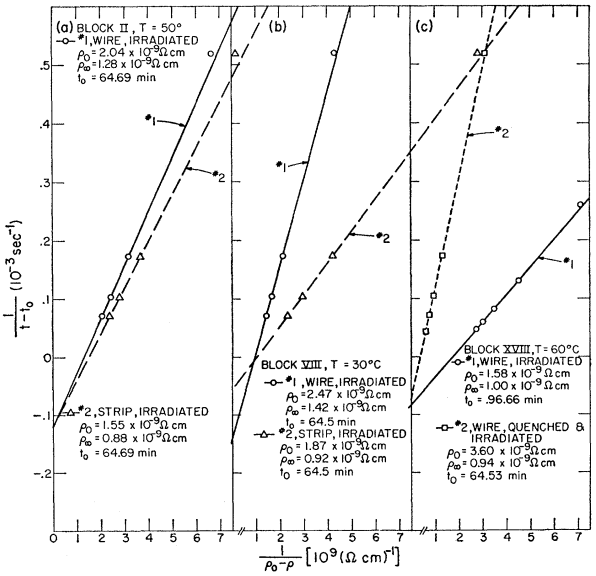

FIG. 7. (a) Second-order fit of the long isothermal for the block II at 50°C. (b) Second-order fit of the long isothermal for the block VIII at 30°C. (c) Second-order fit of the long isothermal for the block XVIII at 60°C.

slightly lower than the activation energies obtained on quenched gold samples by Kino and Koehler[7] (E_{strip} $=0.90\pm0.05$ eV) but lie within the error limit. They are in agreement with the Simmons-Balluffi[8] value of 0.87 ± 0.10 eV for the migration of a vacancy in gold obtained by an equilibrium experiment.

In gold, therefore, one sees the same effective energy of migration in quenched specimens as in 3-MeV electron-irradiated specimens. This suggests that the migration of lattice vacancies is responsible for stage-III annealing in gold. Interstitials and interstitial clusters are not likely in quenched gold so that one can eliminate the suggestion that the migration of an interstitial or of some interstitial cluster results in stage-III annealing. There is growing evidence in electron microscopy[9–18] that interstitial clusters are formed during irradiation at or above the liquid-nitrogen temperature. Recently Duesing, Hemmerich, Meissner, and Schilling[19] have concluded from nitrogen-temperature irradiation that, in platinum, interstitials are well separated and clouded around an impurity without clustering. But this is not the result of direct observation, and as they stated in their paper, this conclusion is a rather rough estimate. Moreover, gold and platinum may be different. Even in the case of gold, if one uses such impure specimens as they used ($\gtrsim 10^{-8}$ Ω cm), cluster size becomes very small to be observed. Indeed, Shimomura's observation[9] shows that the purer the material, the bigger is the cluster size and the smaller the number of clusters.

In order that appreciable annealing of resistivity occur in stage III in gold, it is necessary that vacancy-interstitial annihilation occur during the annealing. The simplest model which achieves this result is one which assumes that vacancies migrate to interstitial clusters where the annihilation occurs, or a vacancy first meets another vacancy forming a divacancy. This divacancy migrates to an interstitial cluster. That divacancy migration is not involved can be seen as follows: As will be shown in Sec. IV C, the number of jumps required for annihilation in an irradiated specimen having a given $\Delta\rho$ is about 50 times smaller than in a quenched specimen having the same $\Delta\rho$. This suggests that the sinks differ in an irradiated sample from those in a quenched specimen and indeed Shimomura's electron microscope pictures[9] support this idea. But such a suggestion implies that at least a considerable fraction of the vacancies actually migrate directly to the sink, since otherwise the sink would not influence the number of jumps to annihilation. This fact implies that the interaction between a single vacancy and an interstitial cluster must be large so that the migration of vacancies is no longer of random nature. This very fact explains why the stage-III annealing temperature in the irradiated specimen is lower than that in the quenched specimen. One can also understand the existence of a shoulder in the stage-III peak for the quench-plus-irradiated specimen [Fig. 3(c)]. Namely, vacancies migrate to interstitial clusters in the lower-temperature part of the peak, and then, since the number of vacancies is larger than the total number of interstitials in the quench-plus-irradiated specimen, all the interstitial clusters are annihilated by migrating vacancies. Thus only vacancies are left behind. The situation thereafter is the same as the case of a quenched specimen. Electron microscopic results by Shimomura show that clusters are present below stage III in gold after electron irradiation.[9] Shimomura observes the annealing out of some of the clusters when the thinned sample is warmed

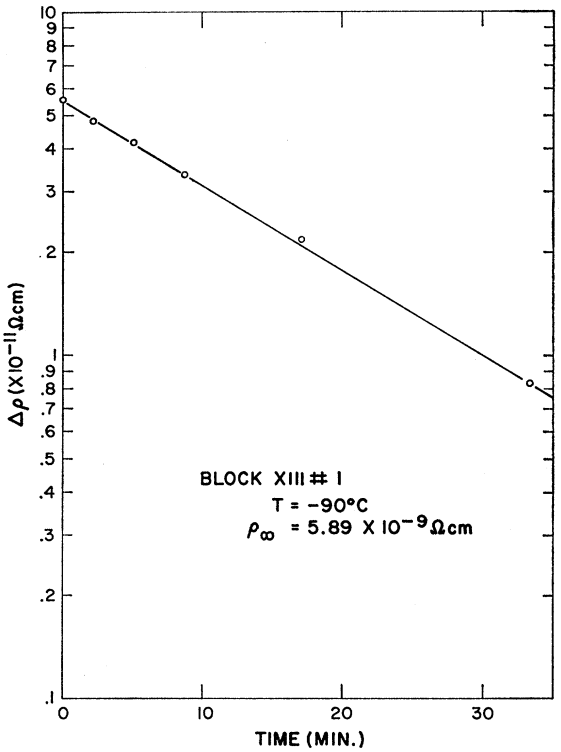

FIG. 8. First-order plot of the specimen XIII-1 (wire, irradiated) at −90°C.

[7] T. Kino and J. S. Koehler, Phys. Rev. **162**, 632 (1967).
[8] R. O. Simmons and R. W. Balluffi, Phys. Rev. **125**, 862 (1962).
[9] Y. Shimomura (to be published). See also Bull. Am. Phys. Soc. **13**, 381 (1968).
[10] D. G. Brandon, P. B. Bowden, and A. J. Baker, in *Properties of Reactor Materials and Effects of Radiation Damage*, edited by D. J. Littler (Butterworths Scientific Publications Ltd., London, 1962), p. 120.
[11] P. Bowden and D. G. Brandon, J. Nucl. Matter **9**, 348 (1963); Phil. Mag. **8**, 935 (1963).
[12] H. Diepers, Phys. Status Solidi **24**, 235 (1967); **24**, 623 (1967).
[13] M. G. McIntyre, Phil. Mag. **15**, 205 (1967).
[14] A. Bourret and D. Dautreppe, Phys. Status Solidi **24**, K173 (1967).
[15] D. J. Mazey and R. S. Barnes, Phil. Mag. **17**, 387 (1968).
[16] L. M. Howe, R. W. Gilbert, and G. R. Piercy, Appl. Phys. Letters **3**, 125 (1963).
[17] R. S. Barnes, G. B. Redding, and A. H. Cottrell, Phil. Mag. **3**, 97 (1958).
[18] R. J. Barnes and D. J. Mazey, Phil. Mag. **5**, 1247 (1960).
[19] G. Duesing, H. Hemmerich, D. Meissner, and W. Schilling, Phys. Status Solidi **23**, 481 (1967).

through stage III. In addition, gold specimens electron-irradiated at 100°K and warmed through stage III before thinning for electron microscopy do not show defect clusters, suggesting that they vanish during stage-III annealing in a thick (but not completely in a thin) specimen. In a thin specimen, clusters do not vanish completely in stage-III annealing because many of the vacancies migrate to the surface.

The data therefore indicate that interstitial clusters are formed during irradiation at 100°K. The interstitial clusters are sufficiently tightly bound that they persist until they are eliminated by the migrating vacancies in stage III.

At this point one might suspect that the vacancy migration to interstitial clusters can not give second-order kinetics. It can be shown that under reasonable conditions this model does give second-order kinetics. Electron microscopy[9] shows that the average disk-shaped interstitial cluster is fairly large in gold (~50 Å). Then we can write the rate equation as follows:

$$\dot{C}_V = -K_1 C_V^2 + K_2 C_{V2} - \sum_n K_{1n} C_{In} C_V, \quad (4.1)$$

$$\dot{C}_{V2} = \tfrac{1}{2} K_1 C_V^2 - \tfrac{1}{2} K_2 C_{V2} - \sum_n K_{2n} C_{In} C_{V2}, \quad (4.2)$$

$$C_V + 2C_{V2} = \sum_n n C_{In}, \quad (4.3)$$

where K_1, K_2, K_{1n}, and K_{2n} are the rate constants for divacancy formation, for divacancy breakup, for single vacancy migration to the cluster of n interstitials, and for the divacancy migration to the cluster of n interstitials, respectively. C_{In} is the fractional concentration of the clusters containing n interstitials, C_V is the vacancy concentration, and C_{V2} is the divacancy concentration. Introduce the resistivity $\Delta\rho$ as

$$\begin{aligned}\Delta\rho &\equiv f_V C_V + f_{V2} C_{V2} + f_I' \sum_n n C_{In} \\ &\equiv f_V C_V + (2f_V - \Delta f) C_{V2} + f_I' \sum_n n C_{In}, \quad (\Delta f > 0) \\ &= f_V (C_V + 2C_{V2}) - \Delta f C_{V2} + f_I' \sum_n n C_{In}.\end{aligned}$$

From Eq. (4.3),

$$\Delta\rho = (f_V + f_I')(C_V + 2C_{V2}) - \Delta f C_{V2}, \quad (4.4)$$

where $f_V/100$, $f_{V2}/100$, and $f_I'/100$ are the resistivities due to 1% of vacancies, of divacancies, and of interstitials within clusters. Thus Eqs. (4.1), (4.2), and (4.4) give

$$\begin{aligned}\Delta\dot{\rho} = &-(f_V + f_I') \sum_n K_{1n} C_{In} C_V \\ &-(2f_V + 2f_I' - \Delta f) \sum_n K_{2n} C_{In} C_{V2} \\ &-\tfrac{1}{2}\Delta f K_1 C_V^2 + \tfrac{1}{2}\Delta f K_2 C_{V2}. \quad (4.5)\end{aligned}$$

The small number of jumps to annihilation in the irradiated specimens (see Sec. IV C) means that a single vacancy is more likely to be annihilated directly at the interstitial cluster rather than meeting another vacancy to form divacancy before annihilation. This together with the fact that the divacancy migration energy is considerably lower than that of a single vacancy leads us to expect the divacancy concentration to be very small compared to the single-vacancy concentration. Equations (4.5) and (4.4) can then be written as

$$\Delta\dot{\rho} = -(f_V + f_I')\left(\sum_n K_{1n} C_{In}\right) C_V - \tfrac{1}{2}\Delta f K_1 C_V^2 \quad (4.6)$$

and

$$\Delta\rho = (f_V + f_I') C_V. \quad (4.7)$$

Thus

$$\Delta\dot{\rho} = -\Delta\rho \sum_n K_{1n} C_{In} - \frac{\Delta f}{2(f_V + f_I')^2} K_1 (\Delta\rho)^2. \quad (4.8)$$

Now define an average rate constant $K_{1\bar{n}}$ as

$$K_{1\bar{n}} = \sum_n K_{1n} C_{In} / \sum_n C_{In},$$

where $\bar{n}$ is the average number of interstitials in a cluster and is given by

$$\bar{n} = \sum_n n C_{In} / \sum_n C_{In}.$$

The electron microscope results of Shimomura[9] on electron-irradiated gold are in agreement with this assumption, i.e., Shimomura finds an average size without too much spread in cluster size.

$$\begin{aligned}\sum K_{1n} C_{In} &= K_{1\bar{n}} \sum C_{In} = (K_{1\bar{n}} \sum n C_{In})/\bar{n} \\ &= (K_{1\bar{n}}/\bar{n}) C_V = [K_{1\bar{n}}/\bar{n}(f_V + f_I')]\Delta\rho. \quad (4.9)\end{aligned}$$

Thus, Eqs. (4.8) and (4.9) give

$$\begin{aligned}\Delta\dot{\rho} &= -\frac{K_{1\bar{n}}}{\bar{n}(f_V + f_I')}(\Delta\rho)^2 - \frac{\Delta f}{2(f_V + f_I')^2} K_1 (\Delta\rho)^2 \\ &= -\frac{(\Delta\rho)^2}{(f_V + f_I')}\left[\frac{K_{1\bar{n}}}{\bar{n}} + \frac{\Delta f K_1}{2(f_V + f_I')}\right]. \quad (4.10)\end{aligned}$$

Thus we obtain the second-order, Arrhenius-type equation. In obtaining above results, we assumed $V_2 \ll V_1$. This condition, however, may not be satisfied too well in general. Then one can expect the deviation from the second-order kinetics which is actually observed at both sides of the stage-III main peak. It is to be noted here that experimentally a quenched specimen follows second-order kinetics more closely than an irradiated specimen. The only other assumption used is that $K_{1\bar{n}}/\bar{n}$ should not vary much with the average size of the interstitial cluster. The strain field, if we think of it as similar to a dislocation loop, gives an interaction potential

$$V = K b_c b_V^3 f(\theta\phi) L^2 / r^3,$$

where K is a constant involving the elastic constants, b_c and b_V are constants (dimensions cm) which measure the "strength" of the cluster strains and the vacancy strains, L is the diameter of the cluster, r is the distance of the vacancy from the cluster, and θ and ϕ give other coordinates of the vacancy relative to the cluster. Thus V, because of the L^2, is proportional to the number n of interstitials in the cluster. Probably a large cluster captures vacancies from a large volume, i.e., $\langle r^3\rangle_{\text{av}}$ is probably proportional to L^2 and hence to n. This arranges matters so that the average vacancy, cluster interaction energy is about the same for all cluster sizes and it also brings in just the correct number of vacancies required to annihilate the cluster.

Since the formation energy of an interstitial is much larger than that of a vacancy, one expects to find vacancies in equilibrium in gold at high temperature. This is what is observed in the Simmons-Balluffi[8] equilibrium experiment on gold. Thus in quenched gold we expect to find lattice vacancies and vacancy clusters, but not interstitials of any kind. Hence it is difficult to understand how interstitial migration or di-interstitial migration can be responsible for stage-III annealing in irradiated gold. These ideas fit the data of Grenning and Koehler,[20] who trapped interstitials at small closed-shell impurities in gold (Al and Mg). The impurities used were chosen to trap interstitials. They found that the stage-III activation energy was lower in impure gold than in pure gold. This is not what one would expect if interstitial migration is responsible for stage III since in the impure gold one would expect an increased annealing energy (i.e., $E_M{}^I+B_{Ii}$, the migration plus the trapping energy).

The interstitial cluster breakup model proposed by Doyama[3] does not give second-order annealing kinetics. Moreover, one would expect this model to give a stage-III activation energy which increases with dose since the size of the cluster increases with dose, contrary to the observed results (Sec. III D 3).

Thus only the vacancies migrating to the interstitial clusters can explain the stage-III experiments on gold.

B. Influence of Purity

The specimen purity plays an important role in the results obtained, although at present not all of the effects are understood.

Consider first the rate of damage production. Let us assume that single interstitials generated during irradiation migrate freely at the irradiation temperature. This postulate is consistent with the fact that the production rate is suppressed remarkably by quenching the specimen before irradiation (see Sec. III A). These migrating interstitials end either by annihilation at a stationary lattice vacancy or by joining an interstitial cluster which is probably initiated at an impurity atom. Then, following the similar treatment by others,[21–23] the rate equations during the irradiation can be written as

$$\dot{C}_I = AF - \sigma K_I C_i C_I - K_I C_I C_V, \tag{4.11}$$

$$\dot{C}_{IC} = \sigma K_I C_i C_I, \tag{4.12}$$

$$\dot{C}_V = AF - K_I C_I C_V. \tag{4.13}$$

Here F is the electron flux, C_i is the fractional concentration of impurities capable of nucleating interstitial clusters, C_I is the mobile interstitial concentration, C_{IC} is the interstitial cluster concentration, C_V is the fractional vacancy concentration, K_I is the rate constant associated with interstitial migration, and σ is the capture volume of the interstitial clusters measured in atomic volume. If we assume a steady state for the interstitials

$$\dot{C}_I = 0,$$

then, from Eq. (4.11), we get

$$C_I = AF/K_I(\sigma C_i + C_V). \tag{4.14}$$

First consider the simplest case in which σ is constant. Then, inserting (4.14) into (4.12) and (4.13) and integrating, one finds

$$C_V = C_{IC}$$

and

$$C_V = -\sigma C_i + [2AF\sigma C_i(t+\sigma C_i/2AF)]^{1/2}.$$

The production of resistivity is then

$$\Delta\rho \equiv (f_V + f_I')C_V \equiv (f_V + f_I') \times\{-\sigma C_i + [2A\sigma C_i(\phi+\sigma C_i/2A)]^{1/2}\}, \tag{4.15}$$

where f_V is the resistivity due to 100% of vacancy concentration, f_I' is the resistivity due to 100% of interstitials in the clusters, and $\phi = Ft$ is the total integrated electron flux. The fit of this expression to the measured data is reasonably good up to the damage of $6\times10^{-9}\ \Omega$ cm.

In fact, the size of interstitial clusters grows during irradiation so that σ becomes larger as time elapses. For simplicity, let us assume that σ grows linearly with vacancy concentration:

$$\sigma = \sigma_0 + \alpha C_V, \tag{4.16}$$

where σ_0 is the value of σ at time $t=0$ and is of the order of unity, and α is a constant. From Eqs. (4.13), (4.14), and (4.16), one gets the relation

$$\frac{\alpha C_i + 1}{\alpha C_i} C_V - \frac{\sigma_0}{\alpha} \ln\left(\frac{\alpha}{\sigma_0} C_V + 1\right) = AFt = A\phi. \tag{4.17}$$

The fit of this result to the experimental results is good up to the damage of $5\times10^{-9}\ \Omega$ cm. The damage-produc-

[20] D. A. Grenning and J. S. Koehler, Phys. Rev. **144**, 439 (1966).

[21] R. M. Walker, in *International School of Physics "Enrico Fermi," Course 18*, edited by D. S. Billington (Academic Press Inc., New York, 1962).

[22] J. W. Corbett and R. M. Walker, Atomic Energy Commission Report No. NAA-SR-3250, 1960 (unpublished).

[23] T. R. Waite, Phys. Rev. **107**, 463 (1957).

tion data for higher dose in the present work is not too reliable. Further work is necessary to clarify which model is best. Equations (4.15) and (4.17) agree qualitatively with those obtained by Walker[21] for the case of unsaturable traps and the case of nucleation traps, respectively.

A second place in which purity plays a role is in the annealing below stage III. This is particularly evident in Fig. 2. The impure gold shows a small annealing peak at -90°C and in addition shows a steady continuous decrease as the annealing temperature is raised. Such a continuous change does not appear to be the usual kind of thermally activated process. It is very suggestive that, when Blewitt *et al.*[24] studied copper containing a small amount of gold, the isochronal curves showed considerable continuous annealing. Further work will be necessary to establish better understanding of the phenomena. In both aluminum[3] and gold, this effect can be minimized by the use of high-purity specimens (Figs. 2 and 3).

The third place in which purity plays a role is in the activation energy seen in stage III. One finds consistently that the activation energy E_{III} increases with increasing purity as measured by the residual resistivity (see Fig. 5). This effect is also seen in quenched specimens,[7,25] indicating that the interstitial clusters may not play a role. There are several possibilities, but further research will be required to decide which is most important. At this point we would like to mention the calculations by de Jong[26] and Koehler and Kino[27] on the impurity effect on the vacancy migration energy.

Finally, the damage remaining in gold after annealing through stage III seems to decrease as the purity increases. In the present work, the remaining damage after stage III is less than 3% for the irradiated specimens with the residual resistivity of $\rho^0 \cong 0.5\times10^{-9}$ Ω cm. (See Sec. III B.) On the other hand, the corresponding figure observed by Bauer and Sosin[2] is about 7% for the specimens with the residual resistivity of $\rho^0 \cong 2.5\times10^{-9}$ Ω cm and with about the same initial damage.

C. Number of Jumps and Capture Volume

The number of jumps to annihilation is given by

$$n_j = t_{1/2}\nu G e^{-E/kT}, \tag{4.18}$$

where $t_{1/2}$ is the time required to anneal out half the damage, ν is the frequency factor, G is the entropy factor, E is the activation energy, k is the Boltzmann constant, and T is the absolute temperature. This number can be determined by finding $t_{1/2}$ from the isothermal data (Figs. 6 and 7). For example, in the case of the irradiated specimen XIV-2, $t_{1/2}=2.56\times10^3$ sec, $E=0.836$ eV, $T=313$°K, and taking $\nu G=3\times10^{13}$ sec^{-1}, we get $n_j=2.7\times10^3$. This number is much lower than one would expect from the random-walk calculation: For fcc metals, the number of jumps required by random-walk calculation[28] is

$$n_j^{\mathrm{calc}} = 1.345/C, \tag{4.19}$$

where C is the fractional concentration of sinks of atomic size and of inexhaustible nature. For the specimen XIV-2 above, $C \cong 1.2\times10^{-5}$ at $T=313$°K, assuming one kind of defect annihilates at the other kind. Then we get $n_j^{\mathrm{calc}}=1.1\times10^5$. Thus the random-walk calculation gives an n_j about 50 times larger than the experimental value for n_j. This discrepancy can be understood if we assume that the annihilation occurs with a large capture volume. This matter will be discussed later in more detail. It is also found that n_j stays fairly constant until the annealing peak temperature is reached and then increases rapidly as the annealing temperature rises.

On the other hand, in the case of the quench-plus-irradiated and quenched specimens, the number of jumps obtained experimentally agrees with that given by the random-walk calculation; e.g., in the case of quenched and irradiated specimen XIV-1, $E=0.861$ eV, $T=363$°K, $t_{1/2}=3.94\times10^3$ sec. Taking $\nu G=3\times10^{13}$ sec^{-1}, we obtain $n_j=1.3\times10^5$, while we get $n_j^{\mathrm{calc}}=1.3\times10^5$ with $C\cong1.0\times10^{-5}$, in agreement with the experimental value. In the case of quenched specimen XI-2, $E=0.856$ eV, $T=363$°K, $t_{1/2}=4.42\times10^3$ sec, and we get $n_j=1.7\times10^5$, in agreement with the calculated value $n_j^{\mathrm{calc}}=1.7\times10^5$ for $C=0.81\times10^{-5}$. These results are tabulated in Table III.

For a second-order process, from Eq. (3.8)

$$(t-t_0)^{-1}=\alpha(\rho_0-\rho_\infty)^{-1}-\beta, \tag{4.20}$$

where

$$B=\sigma\nu G/f, \tag{4.21a}$$

$$\alpha=Be^{-E/kT}(\rho_0-\rho_\infty)^2, \tag{4.21b}$$

$$\beta=Be^{-E/kT}(\rho_0-\rho_\infty). \tag{4.21c}$$

Here σ is the capture volume measured in number of atomic volumes and is a dimensionless quantity, and G is a constant including an entropy factor. From Eq. (4.21),

$$\beta^2/\alpha = Be^{-E/kT}$$

or

$$B=(\beta^2/\alpha)e^{E/kT}. \tag{4.22}$$

α and β can be obtained from the graph of the second-order plot (Figs. 6 and 7). Therefore we can find a modified frequency factor B, which gives the value of σ using Eq. (4.21a). For example, in the case of the specimen XIV-2, $\alpha=4.562\times10^{-13}$ Ω cm/sec, $\beta=0.390$

[24] T. H. Blewitt, R. R. Coltmann, C. E. Klabunde, and T. S. Noggle, J. Appl. Phys. **28**, 639 (1957).
[25] R. K. Sharma, C. Lee, and J. S. Koehler, Phys. Rev. Letters **19**, 1379 (1967).
[26] M. de Jong, Phil. Mag. **11**, 1189 (1965).
[27] J. S. Koehler and T. Kino, J. Phys. Chem. Solids **28**, 317 (1967).
[28] See, for example, A. C. Damask and G. J. Dienes, *Point Defects in Metals* (Gordon and Breach, Science Publishers, Inc., New York, 1963), p. 82.

TABLE III. Number of jumps and capture volume ($\nu G=3\times10^{13}$ sec^{-1}).

Specimen	Temperature T (°C)	Concentration at T	E (eV)	$\sigma\nu G/f$ $(\Omega$ cm sec$)^{-1}$	Capture[a] volume σ	n_j	n_j[calc b]	Remarks
XIV-2	40	1.2×10^{-5}	0.836	9.5×10^{18}	64	2.7×10^{3}	1.1×10^{5}	strip, irrad.
XIV-1	90	1.0×10^{-5}	0.861	1.3×10^{17}	0.9	1.3×10^{5}	1.3×10^{5}	strip, quench+irrad.
XI-2	90	0.81×10^{-5}	0.856	1.5×10^{17}	1.0	1.7×10^{5}	1.7×10^{5}	strip, quench
XXI-1	40	1.9×10^{-5}	0.851	6.6×10^{18}	44	1.4×10^{3}	7.1×10^{4}	strip, irrad.
VIII-2	40	0.65×10^{-5}	0.850	4.6×10^{18}	31	9.5×10^{3}	2.1×10^{5}	strip, irrad.

[a] Assume $f=2.0\times10^{-4}$ Ω cm.
[b] Random-walk calculation assuming atomic size sink.

$\times10^{-3}$ sec^{-1}, $E=0.836$ eV, $T=313$°K. These values give $B=9.53\times10^{18}$ $(\Omega$ cm/sec$)^{-1}$. Then, taking $\nu G=3\times10^{13}$ sec^{-1} and $f=2.0\times10^{-4}$ Ω cm, Eq. (4.21a) gives $\sigma=63.7$. The capture volume and the modified frequency factor B for various specimens are listed in Table III.

The values in Table III show a remarkable difference between the irradiated specimens and the quenched ones: For the quenched (or quench-plus-irradiated) specimen, the capture volume is of the order of 1, and the number of jumps determined by experiment agree with that given by a random-walk calculation. On the other hand, the capture volume for the irradiated specimen, the capture volume is large (30–60) and the number of jumps obtained by experiment is much smaller than that given by random-walk calculation. These facts, together with the marked difference in the frequency factor A/f in the Primak analysis (Sec. III D 3), indicate the completely different type of sink in the two different cases. (See Sec. IV A.)

In the case of a quenched specimen, the small capture volume of the order of unity and the fact that the observed number of jumps is the same as that by a random-walk calculation means that the annihilation of defects occurs by the migration of a point defect to another point defect. What is most likely is that vacancies migrate to another vacancy, forming a divacancy. These tightly bound divacancies then migrate to a vacancy tetrahedron which originally nucleated at an impurity or an impurity cluster.

The fact that the number of jumps is anomalously small in irradiated specimens, but not in quenched samples, implies that in the irradiated specimens single vacancies migrate to interstitial clusters rather than to other vacancies to form divacancies. The number of jumps is low because the vacancy diffusion occurs in the stress field of the interstitial cluster and is thus not a random walk. This interpretation implies that the stage-III peak width should be larger in irradiated than in quenched specimens. The isochronal experiments verify this: The peak half-width on the irradiated specimen XIII-1 having $\Delta\rho_R=5.20\times10^{-9}$ Ω cm is about 60°C, whereas the half-width on the quenched specimen with $\Delta\rho_Q=2.71\times10^{-9}$ Ω cm is 50°C. (See Fig. 3.) The theoretical peak half-width[29] should be 35°C so that even in the quenched specimen the peak width is too large. This is not surprising since even in a quenched sample some interaction with the vacancy tetrahedra should be expected.

It is important to notice that the model used here implies that the interstitials are tightly bound in an interstitial cluster. If we assume that the interstitial migration energy $E_M{}^I$ is small (of the order of 0.05 eV), then, since vacancies move before interstitial clusters break up, we must require that

$$B_I+E_M{}^I\geq0.85\text{ eV}.$$

Thus the binding energy of an interstitial to a cluster must exceed 0.8 eV.

D. Models for Other Metals

As discussed in Sec. IV B, it is likely that in the case of pure gold vacancies migrate directly to interstitial clusters giving annihilation. It is important to consider whether other metals are similar.

Let us first consider the case of aluminum. Lwin, Doyama, and Koehler[3] obtained the result $E_{III}=0.62\pm0.04$ eV for the electron-irradiated pure aluminum. Federighi *et al.*[30] also obtained $E_{III}=0.62\pm0.02$ eV. These values agree well with the effective migration energy of quenched-in defects (mostly single vacancy) which is reported to be 0.61 ± 0.04 eV in the case of low defect concentration and high annealing temperature.[31–34] This indicates that vacancy migration is also responsible for stage-III annealing in aluminum.

In the case of copper and silver, the picture is not so clear. From the equilibrium defect experiments, Simmons and Balluffi[35,36] obtained the vacancy migration

[29] See, for example, V. Vand, Proc. Phys. Soc. (London) **A55**, 222 (1943); or R. O. Simmons, J. S. Koehler, and R. W. Balluffi, in *Radiation Damage in Solids* (International Atomic Energy Agency, Vienna, 1962).
[30] T. Federighi, S. Ceresara, and F. Pieragostini, Phil. Mag. **12**, 1093 (1965).
[31] W. De Sorbo and D. Turnbull, Acta Met. **7**, 83 (1959); Phys. Rev. **115**, 560 (1959).
[32] C. Panseri and T. Federighi, Phil. Mag. **3**, 1223 (1958).
[33] C. Panseri, S. Ceresara, and T. Federighi, Nuovo Cimento **29**, 1223 (1963).
[34] M. Doyama and J. S. Koehler, Phys. Rev. **134**, A522 (1964).
[35] R. O. Simmons and R. W. Balluffi, Bull. Am. Phys. Soc. **7**, 233 (1962).
[36] R. O. Simmons and R. W. Balluffi, Phys. Rev. **119**, 600 (1960).

energy of 0.88±0.13 eV for copper and 0.82±0.11 eV for silver. Doyama and Koehler[37] obtained $E_M{}^V=0.83\pm0.05$ eV from a quenching experiment on silver. On the other hand, the stage-III activation energy after 10-MeV proton irradiation was reported by Dworschak, Herschbach, and Koehler[1] to be $E_{III}=0.71\pm0.04$ eV for copper and $E_{III}=0.67\pm0.03$ eV for silver. Thus, stage-III activation energies are much lower than the vacancy migration energies for these metals. There are two possibilities: (a) Either the stage-III activation energy is lowered by some effect (e.g., impurity effect) or (b) the annealing mechanism in Cu and Ag is different from that of Au and Al.

E. Size Effect

It should be noted that the size effect due to the surface scattering becomes more and more important as the purity of the specimen goes higher. Theoretical equations for the size effect were derived by Fuchs[38] for the thin foil and by Dingle[39] for wires. The effect has been discussed extensively by Sondheimer.[40] There are several experimental measurements[41–44] which confirm the theory. The theory in general fits fairly well to the experimental results, assuming completely diffuse scattering at the surface.

Experimental values obtained so far for the product of bulk resistivity and the mean free path are not too accurate, especially for gold. Fortunately, however, the effects of size correction to the experimental results obtained in the present work are rather small. First, size correction gives practically no change in the activation energies obtained in the present experiment. This is due to the fact that the ratio of the change in resistivity of the real specimen to the change in resistivity of the bulk material is much smaller than the ratio of the resistivity of the actual specimen to the resistivity of the bulk materials for a given value of κ (κ=ratio of thickness to the bulk mean free path). Theoretically, the activation energy obtained by the slope-change method should not be affected by size correction since the slopes are changed by the same factor for a given value of κ. This fact is confirmed experimentally using the data obtained in the present work.

The size effect on the order of kinetics is also found to be small for the rather short annealing time (less than 300 min) in the present work. But the size correction may alter somewhat the shape of a very long isothermal annealing curve taken on a high-purity specimen. Thus if one tries to use Meechan-Brinkmann method of analysis to obtain an activation energy for very pure material, care must be taken in the interpretation of results.

V. SUMMARY AND CONCLUSIONS

The following are the results and conclusions obtained in this experiment:

(i) The activation energy of stage-III annealing for the electron-irradiated gold is 0.85±0.02 eV for strip specimens and 0.83±0.03 eV for wire specimens. This agrees with the migration energy of a single vacancy as measured in quenched specimens within experimental error. The change-of-slope method and Primak analysis both give the same activation energy for stage-III annealing of electron-irradiated gold.

(ii) The main part of stage-III annealing obeys second-order kinetics for the irradiated, the quench-plus-irradiated, and quenched specimens.

(iii) The stage-III activation energy increases as the specimen purity increases.

(iv) The damage production at liquid-nitrogen temperature is enhanced by the presence of impurities and the production curve bends down as the dose increases. The damage-production rate is suppressed remarkably by prequenching the specimen before irradiation. This shows that interstitials migrate at the irradiation temperature.

(v) Stage-III annealing occurs by lattice-vacancy migration. The difference in number of jumps between quenched and irradiated samples establishes that single vacancies migrate to interstitial clusters moving in the stress field of the cluster.

(vi) The size correction gives little change in the results found in the present work.

ACKNOWLEDGMENTS

We would like to thank Dr. Y. Shimomura for the opportunity to see and discuss his electron miscroscope pictures before publication. We would also like to thank W. Schooley and B. Clymer for their help with Van de Graaff irradiations. Finally, we would like to thank R. Berliner for assistance with measurements and calculations.

[37] M. Doyama and J. S. Koehler, Phys. Rev. **127**, 21 (1962).
[38] K. Fuchs, Proc. Camb. Phil. Soc. **34**, 100 (1938).
[39] R. B. Dingle, Proc. Roy. Soc. (London) **A201**, 545 (1950).
[40] E. H. Sondheimer, Advan. Phys. **1**, 1 (1952).
[41] E. R. Andrew, Proc. Phys. Soc. (London) **A62**, 77 (1949).
[42] R. G. Chambers, Proc. Roy. Soc. (London) **A215**, 481 (1952).
[43] K. Forsvoll and I. Holmech, J. Appl. Phys. **34**, 2230 (1963).
[44] F. Dworschak, H. Schuster, H. Wollenbergen, and J. Wurm, Phys. Status Solidi **21**, 741 (1967).